

Article

A Membrane Reactor with Microchannels for Carbon Dioxide Reduction in Extraterrestrial Space

Deqiang Feng, Wenjun Jiang *, Ce Zhang, Long Li, Botao Hu, Jian Song and Wei Yao *

Qian Xuesen Laboratory of Space Technology, China Academy of Space Technology, 104 Youyi Road, Beijing 100094, China; fengdeqiang@qxslab.cn (D.F.); zhangce@qxslab.cn (C.Z.); lilong@qxslab.cn (L.L.); hubotao@qxslab.cn (B.H.); songjian@qxslab.cn (J.S.)

* Correspondence: wenjunjiang@qxslab.cn (W.J.); weiyao@qxslab.cn (W.Y.)

Abstract: Long-term continuous oxygen supply is of vital importance during the process of space exploration. Considering the cost and feasibility, in situ resource utilization (ISRU) may be a promising solution. The conversion of CO₂ to O₂ is a key point for ISRU. In addition, the utilization of the abundant CO₂ resources in the atmosphere of Mars is an important topic in the field of manned deep space exploration. The Sabatier reaction, Bosch reaction, and solid oxide electrolysis (SOE) are well-known techniques for the reduction of CO₂. However, all the above techniques need great energy consumption. In this article, we designed an electrochemical membrane reactor at room temperature based on microfluidic control for the reduction of CO₂ in extraterrestrial space. In this system, H₂O was oxidized to O₂ on the anode, while CO₂ was reduced to C₂H₄ on the cathode. The highest Faraday efficiency (FE) for C₂H₄ was 72.7%, with a single-pass carbon efficiency toward C₂H₄ (SPCE-C₂H₄) of 4.64%. In addition, a microfluidic control technique was adopted to overcome the influence of the microgravity environment. The study may provide a solution for the long-term continuous oxygen supply during the process of space exploration.

Keywords: microchannel; carbon dioxide reduction; membrane reactor; extraterrestrial space



Citation: Feng, D.; Jiang, W.; Zhang, C.; Li, L.; Hu, B.; Song, J.; Yao, W. A Membrane Reactor with Microchannels for Carbon Dioxide Reduction in Extraterrestrial Space. *Catalysts* **2022**, *12*, 3. <https://doi.org/10.3390/catal12010003>

Academic Editors: Shangqian Zhu, Qinglan Zhao and Yao Yao

Received: 19 November 2021

Accepted: 19 December 2021

Published: 21 December 2021

Publisher's Note: MDPI stays neutral with regard to jurisdictional claims in published maps and institutional affiliations.



Copyright: © 2021 by the authors. Licensee MDPI, Basel, Switzerland. This article is an open access article distributed under the terms and conditions of the Creative Commons Attribution (CC BY) license (<https://creativecommons.org/licenses/by/4.0/>).

1. Introduction

In the process of manned space flight and extraterrestrial exploration, astronauts are faced with basic material and energy requirements. An astronaut consumes about 820–840 g of oxygen and exhales 1000–1040 g of carbon dioxide a day [1]. It is expensive and technically difficult to carry all the consumables from Earth for long-term manned extraterrestrial exploration. Therefore, extraterrestrial resources must be utilized and recycled, which could reduce the mass of consumables carried from Earth and make the manned deep space exploration missions feasible. In addition, CO₂ is a metabolic product of humans, which may take a toll on health when the concentration of CO₂ is greater than 4 mmHg [2]. It is of vital importance to reduce CO₂ and produce O₂ and carbon fuels. Up to now, there are several technical paths to achieve this goal. The Sabatier reaction is one of the state-of-the-art CO₂ reduction technologies, which has been fully operational on the International Space Station in 2011 [3]. For the Sabatier reaction, CO₂ is reduced by hydrogen to generate methane and H₂O. Hydrogen comes from water electrolysis. Bosch reaction is another technique for CO₂ reduction, in which CO₂ is reduced by hydrogen to generate carbon and H₂O. Compared with the Sabatier reaction, the Bosch reaction theoretically allows for 100% O₂ recovery from CO₂. However, carbon deposition may block the catalyst surface and reduce reaction efficiency. Solid oxide electrolysis (SOE) provides a direct path for CO₂ decomposition, which could directly split CO₂ into O₂ and CO and is especially of interest for the utilization of CO₂ in the Martian atmosphere [4,5]. The Mars Oxygen In situ Resource Utilization Experiment (MOXIE) has realized the goal of producing O₂ from CO₂ of the Martian atmosphere through SOE, whose oxygen production rate is 5.4 g/h. Despite the remarkable achievements of these technologies, there are also

several obvious drawbacks. For example, hydrogen is necessary for both the Sabatier and Bosch reactions, which may be an unsafe factor for manned aircraft. Moreover, all three reactions are high-temperature reactions (300–800 °C), which heavily consume energy and are unsafe. Therefore, it is urgent to solve these problems through new technology.

Extraterrestrial artificial photosynthesis technology (extraterrestrial photo/electrocatalytic carbon dioxide reduction technology) is a new technology first proposed by Qian Xuesen Laboratory of Space Technology and Nanjing University, which enables the controlled conversion of carbon dioxide into oxygen and carbon-containing fuels through photo/electrocatalysis at room temperature and pressure [6]. Considering that sunlight is almost the only sustainable energy source in extraterrestrial space, the technological path of photovoltaic–electrochemical (PV–EC) may be the optimal technology path for CO₂ utilization, of which zero-gap configuration or membrane electrode assembly (MEA) configuration is most likely to be put into practical application. Although a series of works related to MEA have been reported [7–14], factors related to the reactor adaptability in extraterrestrial space, such as the microgravity environment, mechanics, and airtightness requirements, are rarely considered.

Generally, the CO₂ chemical reduction comprises three steps: CO₂ adsorption, CO₂-to-hydrocarbon conversion, and reaction products separation. First, CO₂ molecules adsorb on the surface of a photocatalyst; then, the electrons migrate from the bulk to the surface to reduce CO₂ to hydrocarbons; lastly, the products desorb and separate from the electrode surface for the sequential reaction. Nevertheless, for the third step, the reaction products, especially gas bubbles, cover the electrode surface and cannot desorb and separate in the microgravity environment, which enlarges the ohmic resistance of the system and even terminates the reaction [15]. Recently, a new technology of microfluidics has emerged, which can leverage specific advantages in photoelectrochemical catalysis such as fine flow control and large surface-area-to-volume ratio. Owing to these features, it has shown great potential to accelerate reaction rates by improving the mass and photon transfer and, hence, has become a promising platform for catalytic reaction systems. Furthermore, the surface tension and flow shear force in the microchannel fluid reaction process could be precisely controlled by adjusting the surface morphology and flow rate to effectively promote the gas–liquid interfacial phase separation under a microgravity environment [16].

Herein, we designed a membrane reactor with microchannels for the electrocatalytic reduction of CO₂ at room temperature in extraterrestrial space. Microfluidic control technique was adopted to overcome the influence of the microgravity environment. In this system, the highest Faraday efficiency (FE) of C₂H₄ was 72.7%, with a current density of 88 mA/cm². The single-pass carbon efficiency (SPCE) of CO₂ toward C₂H₄ and gas products were 4.64% and 11.61%, respectively. In addition, the influence of cell voltage, the flow rate of electrolyte and CO₂, channel structure, and membrane on the reaction are discussed in detail. The study contributes to the long-term, continuous oxygen supply during the process of space exploration.

2. Results and Discussion

2.1. System and Reactor Structure

The schematic of the extraterrestrial artificial photosynthesis system is shown in Figure 1. System components were connected using polyether ether ketone (PEEK), having an outer diameter of 3 mm. In the microgravity environment, liquid cannot be separated effectively from gas and be driven to flow by gas in a conventional container. Thus, in the system, the anolyte was stored in a cystic electrolyte tank of which shell was fabricated with titanium alloy (Aerospace class). The anolyte pressure and flow rate were controlled by a pressure relief valve (Aerospace class). The cathodic gas pressure and flow rate were controlled using a mass-flow controller (CS200A, Beijing Sevenstar Flow Co., Ltd., Beijing, China). Both the anolyte and cathodic gas were connected to the CO₂ gas cylinder, and the circulation was turned on or turned off by controlling the pressure transducers (Aerospace class), of which the on/off threshold pressure values were logged in by the computer, up-

stream of the pressure relief valve and mass-flow controller. Two soft bags manufactured with the polyvinyl chloride (PVC) downstream of the cell were utilized to collect the anodic and cathodic reaction products. The gaseous components of the reaction products were injected into gas chromatography to analyze the gas composition. A high-resolution charge-coupled device (CCD) camera was used to observe and record the gas behavior during the reaction process.

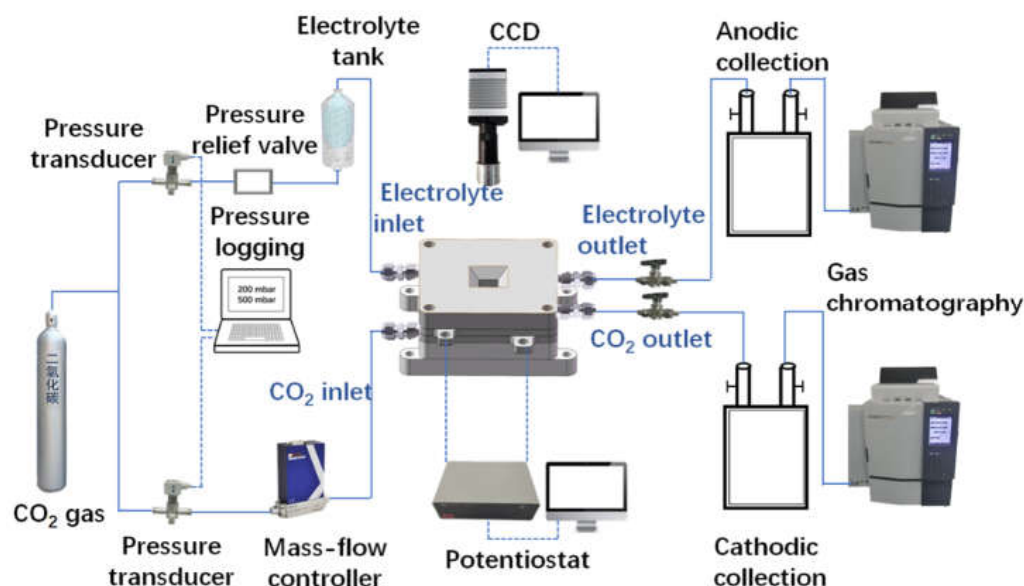
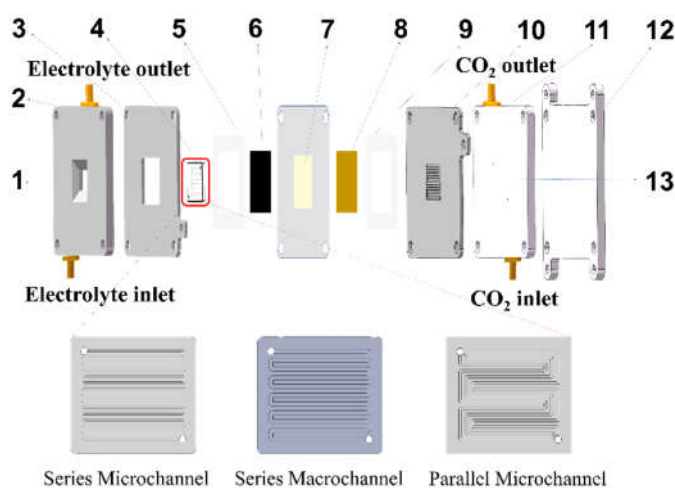


Figure 1. Schematic diagram of the extraterrestrial artificial photosynthesis system.

As shown in Figure 2, all CO₂ electrochemical reduction experiments were performed in a membrane reactor with microchannels, wherein a polymer electrolyte membrane (anion exchange membrane) separates the anode from the cathode. The cathode was exposed to the CO₂ gas stream on one side and the anolyte stream on the other. The IrO₂ anode was completely immersed in the liquid anolyte. The cell contained four inlets and outlets, two ports for each fluid (anolyte and CO₂). To avoid the electrochemical corrosion to the electrode substrate during the reduction process, the cell structure employed electrode substrate and collection substrate as the current collectors and reactant collectors. The anodic and cathodic substrates (current collectors) were fabricated from T4c titanium alloy, wherein the flow field in the center of the anodic substrate was fabricated from transparent polymethylmethacrylate (PMMA) to facilitate observation and recording using a CCD camera. Both flow fields of anodic and cathodic substrates have active areas of $2.5 \times 2.5 \text{ cm}^2$. Considering the influence of microgravity on the separation of gas and liquid, a series microchannel structure and a parallel microchannel structure with a width-to-depth ratio of $600 \mu\text{m}$ to $200 \mu\text{m}$ were utilized during the CO₂ reduction experiments. Moreover, for comparison, a series macrochannel structure with a width-to-depth ratio of $1000 \mu\text{m}$ to $400 \mu\text{m}$ was also investigated. The collection substrate (reactant collectors) and the fixed substrate were fabricated from aluminum metal. In addition, a window on the anodic collection substrate was formed for observation and recorded using a CCD camera.



1-Observation Window, 2, 11-Anodic and Cathodic Collection Substrate, 3-Anodic Substrate, 4, 13-Anodic and Cathodic Microchannel, 5, 9-Gasket, 6-Anode, 7-Membrane, 8-Cathode, 10-Cathodic Substrate, 12-Fixed Substrate

Figure 2. Assembly drawing of the membrane reactor with microchannels.

2.2. Morphology and Structure Characterization

To explore the morphology of CuNWs, scanning electron microscopy (SEM) and transmission electron microscopy (TEM) were carried out. As shown in Figure 3a,b, the morphology of the CuNWs was ultralong nanowires, the length of which was up to around 15 μm . It is worth noting that there was also a small number of nanocubes. Figure 3e and Figure S1 show that the diameter of the CuNWs was around 20~80 nm. Figure 3c,d show the cross-sectional SEM images of the CuNW-based gas diffusion electrode. The gas diffusion electrode (GDE) was composed of the catalyst layer and gas diffusion layer. The thickness was in a range of tens to hundreds of nanometers. The CuNW-based gas diffusion electrode showed a rusty red color (Figure 3f).

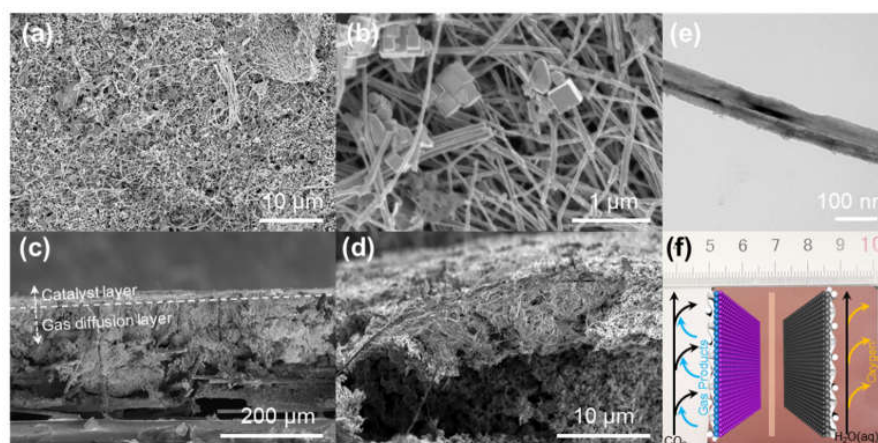


Figure 3. (a,b) SEM images and (c,d) cross-sectional SEM images of CuNW-based gas diffusion electrode; (e) TEM image of CuNWs; (f) photograph and schematic diagram of CuNW-based gas diffusion electrode.

X-ray diffraction (XRD) patterns were performed to elucidate the crystal structure of CuNWs (Figure 4). Three peaks were found at 43.3° , 50.4° , and 74.1° in the XRD patterns, demonstrating that CuNWs displayed a cubic phase of copper sharing a space group of Fm-3m (JCPDS, No. 04-0836). Peaks at 26.8° and 54.4° were ascribed to the carbon paper substrate.

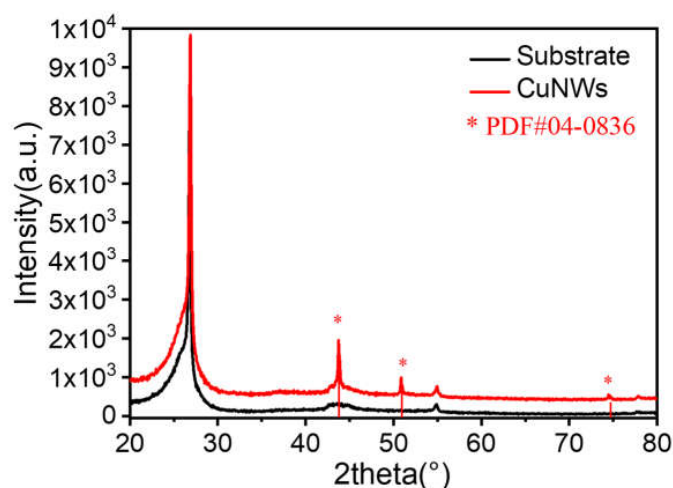


Figure 4. XRD patterns of CuNWs.

X-ray photoelectron spectra (XPS) were conducted to elucidate the surface valence of CuNWs. XPS survey spectrum showed that the samples were composed of Cu, O, and C elements (Figure S2). The peak at 284.8 eV was attributed to the carbon contaminations in the high-resolution XPS spectrum of C1s (Figure 5a) [17]. For the high-resolution XPS spectrum of O1s (Figure 5b), two peaks at 531.8 eV and 529.8 eV were found, which were ascribed to surface adsorbed oxygen and lattice oxygen species, respectively [18]. The Cu2p_{3/2} spectra were deconvoluted to two peaks at 934.2 eV and 932.1 eV (Figure 5c), which were attributed to Cu (II) and Cu (I or 0), respectively [18]. It is difficult to distinguish Cu (I) and Cu (0) through Cu2p since their similar energy values. As shown in Figure 5d, X-ray Auger Cu LMM spectra were adopted to identify Cu (I) and Cu (0). Two peaks were found at 918.4 eV and 916.8 eV, which were ascribed to Cu (0) and Cu (I), respectively [19,20]. Combining the results of XRD and XPS, we can confirm that the Cu element on the surface was mainly in the form of Cu (II) and Cu (I), while the Cu element in the bulk was Cu (0). The possible reason could be attributed to partial oxidation of the surface by the oxygen in the atmosphere.

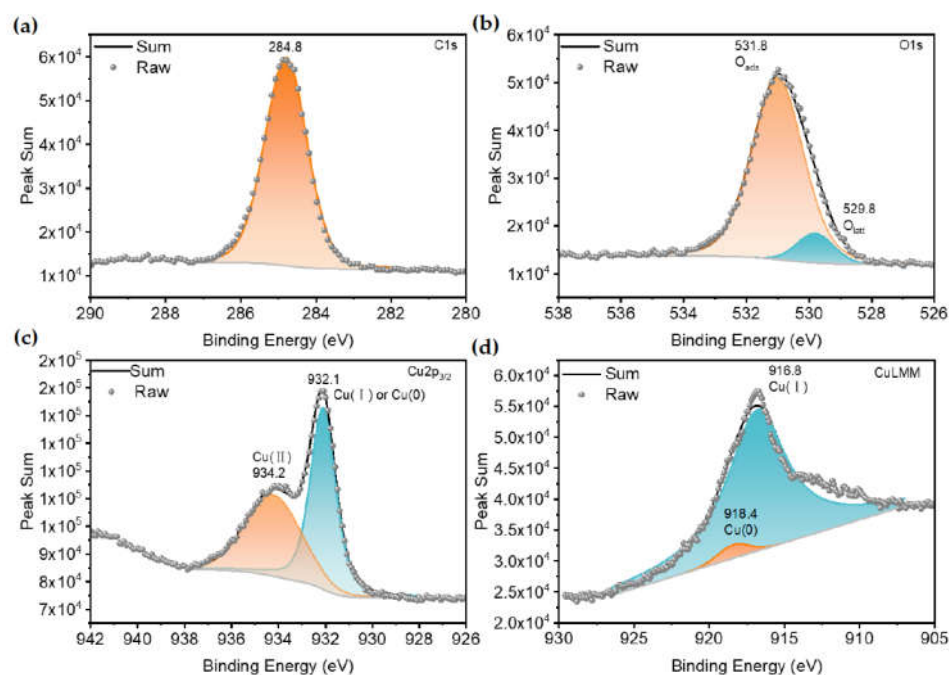


Figure 5. XPS spectra of CuNWs for (a) C1s, (b) O1s, (c) Cu2p_{3/2} and (d) CuLMM.

2.3. CO₂ Reduction Performance

2.3.1. Voltage

KOH solution could provide a strong alkaline environment, which could inhibit hydrogen evolution reaction, strengthen the C–C coupling, and promote the Faraday efficiency (FE) of C₂H₄ [21]. However, the strong alkaline environment will lead to the reaction between CO₂ and OH[−] to form CO₃^{2−}, which could pass through the anion exchange membrane, resulting in cross-contamination, and dragging down the energy efficiency and raw material utilization rate [22,23]. Sargent pointed out that more than 50% of the energy used in the electroreduction of CO₂ under alkaline conditions is used to recover the CO₂ forming CO₃^{2−} [24]. Therefore, a weak alkaline environment may be an effective method of solving this problem. Here, 0.2 M KHCO₃ dilute solution was adopted as the electrolyte solution. As shown in Figure 6a,b, the current increased as the cell voltage increased. The current density reached about 96 mA/cm² when the cell voltage was 4.4 V. Figure 6b shows the Faraday efficiencies (FE) at different cell voltages. The FE of CO decreased as the cell voltage increased, while the FE of C₂H₄ increased as the cell voltage increased. The FEs of C₂H₄ at 4.2 V and 4.4 V were 44.2% and 44.7%, respectively. The highest FE of all gas products for CO₂ reduction (CO₂RR(gas)) reached 61.8% at 4.2 V.

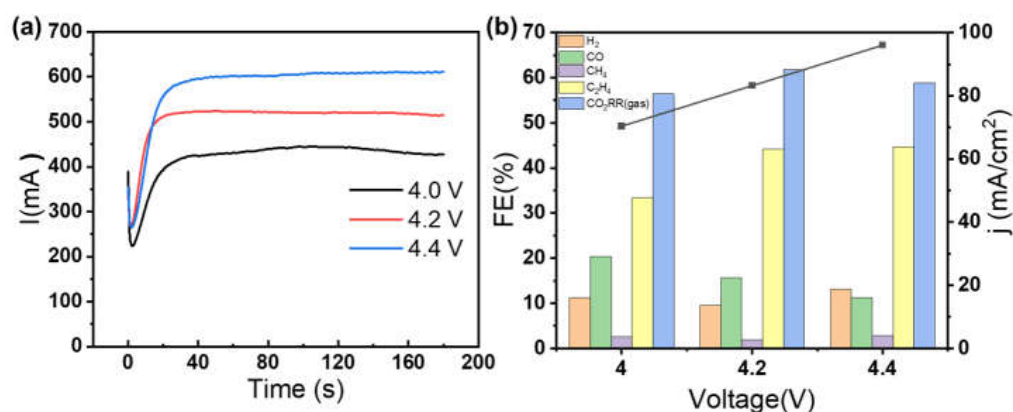


Figure 6. (a) I–t curve at different voltages; (b) the Faraday efficiency of gas products and current density at different voltages. Operating parameter: CO₂ gas flow rate of 20 sccm, anolyte flow rate of 10 sccm, the anion exchange membrane of Sustainion X37-50 Grade T, and the channel type of parallel microchannel structure.

2.3.2. Flow Rate

Furthermore, we explored the influence of the flow rates of electrolyte and CO₂ on the Faraday efficiency of gas products and current density. As shown in Figure 7a, both the FE of C₂H₄ and CO₂RR(gas) increased as the electrolyte flow rate increased. In addition, the FE of H₂ remarkably increased when the electrolyte flow rate was only 5 sccm, which may be ascribed to the bubble accumulation on the electrode surface. Low electrolyte flow rate makes it difficult for O₂ bubbles produced on the electrode to desorb, which leads to higher interface resistance. This phenomenon is magnified in a microgravity environment, which has been proved by Y. Fukunaka [15]. Therefore, it is necessary to keep a relatively high electrolyte flow rate especially in microgravity environment. However, the electrolyte flow rate cannot increase indefinitely considering the reserve of electrolytes in the cystic tank for the entire experiment in an extraterrestrial environment. As shown in Figure 7b, the FE of CO decreased as the gas flow rate decreased, while the FE of H₂ increased as the gas flow rate decreased. The FE of C₂H₄ exhibited a peak value of 67.7% when the gas flow rate was 10 sccm. This phenomenon could be attributed to the increased retention time of *CO since a longer retention time is beneficial for C–C coupling. On the other hand, a low gas flow rate led to low carbon dioxide flux, which is relatively favorable for hydrogen evolution reactions. Combined with the above analysis, the optimal values for electrolyte flow rate and gas flow rate were 10 sccm and 10 sccm, respectively.

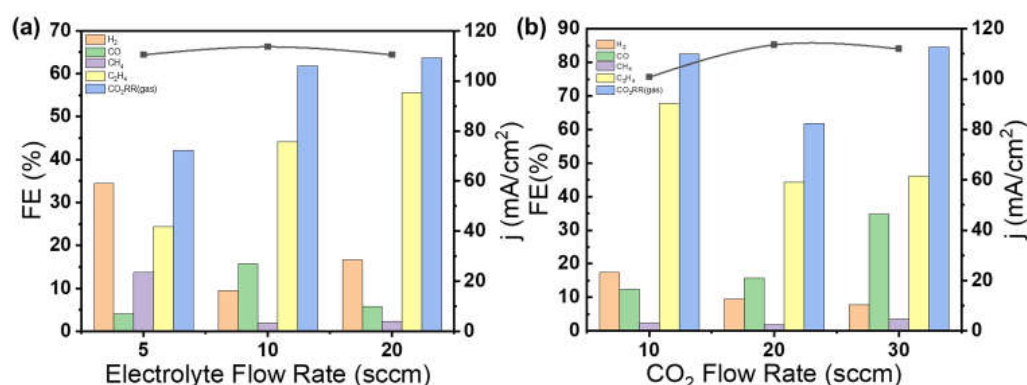


Figure 7. (a) The Faraday efficiency of gas products and current density at different electrolyte flow rates. Operating parameter: Cell voltage 4.2 V, CO₂ gas flow rate of 20 sccm, the anion exchange membrane of Sustainion X37-50 Grade T, and the channel type of parallel microchannel structure; (b) the Faraday efficiency of gas products and current density at different CO₂ flow rates. Operating parameter: Cell voltage 4.2 V, anolyte flow rate of 10 sccm, the anion exchange membrane of Sustainion X37-50 Grade T, and the channel type of parallel microchannel structure.

2.3.3. Channel Structure

Channel structure has an important influence on the distribution of the CO₂ flow field [25]. We designed three types of channel structure to explore the effect of mass transfer on CO₂ reduction reaction: series macrochannel, series microchannel, and parallel microchannel. As shown in Figure 8a, compared with the series macrochannel structure, in the series microchannel, the FE of CO decreased, while the FE of H₂ and C₂H₄ increased, and the FE of C₂H₄ exhibited a value of 54.4%. Particularly, the current density in the series microchannel structure was 88 mA/cm², which is 19.6% higher than that in the series macrochannel model. To explore the reason for the increased current density, we took the microscopy images of the bubble dynamics, shown in Figure 8b. In the series macrochannel model, the O₂ bubble showed a continuous big bubble form. There were two defects in the form. Firstly, the continuous big bubble form would insulate the electrolyte from the electrode, which results in an increased interface resistance and reduced reaction current density. Second, in a microgravity environment, it is difficult for the continuous, large bubble to detach from the electrode, which will further block the reaction. On the contrary, in the series microchannel structure, the O₂ bubble showed a slug flow form. The discontinuous, small bubble could be forced out by the fluid shear stress [16], which may overcome the adverse effect of microgravity on bubble detachment. Compared with the series microchannel model, in the parallel microchannel, the FE of C₂H₄ further increased. The FE of C₂H₄ exhibited a value of 67.7%, and the corresponding current density was 100.8 mA/cm². The increased C₂H₄ FE and current density may be attributed to the strengthened mass transfer of CO₂ [25]. The retention time of CO₂ and *CO in the parallel microchannel structure was longer than that in the series microchannel since the parallel microchannel structure holds a shorter channel length, and a longer retention time strengthens the mass transfer of CO₂ for making the C–C coupling.

2.3.4. Membrane

The thickness, conductivity, and composition of the membranes have important effects on the FE, current density, and even the stability of the CO₂ reduction reaction [26,27]. Here, we compared three common commercial anion exchange membranes: Sustainion X37-50 Grade T (~50 μm, Dioxide Materials, Boca Raton FL, USA), Sustainion X37-50 Grade 60 (~50 μm, Dioxide Materials, Boca Raton FL, USA), and Fumasep FAA-3-20 (~20 μm, Fumatech BWT GmbH, Baden-Württemberg, Germany). The membrane of Sustainion X37-50 Grade T is a sandwich structure with a thin and porous PTFE layer coated. Therefore, the mechanical property is superior. However, as shown in Figure 9, the FE of C₂H₄ using Sustainion X37-50 Grade T is smaller than that using the other two membranes. The FEs

of C_2H_4 and $CO_2RR(gas)$ using Sustainion X37-50 Grade 60 were higher than those using FAA-3-20. The highest FE of C_2H_4 using Sustainion X37-50 Grade 60 was 72.7%, with a current density of 88 mA/cm^2 . The typical TCD and FID chromatograms of cathodic gas products were shown in Figure S3. Table S1 shows the single-pass carbon efficiency (SPCE) of CO_2 in each product at 4.2 V. The SPCE- C_2H_4 and SPCE-gas using Sustainion X37-50 Grade 60 were 4.64% and 11.61%, respectively. The energy efficiency (EE) of CO_2 toward C_2H_4 using Sustainion X37-50 Grade 60 at 4.2 V was 19.9% (Table S2). Evidently, the energy efficiency was relatively low. The reason may be ascribed to the anode, which needs a relatively high overpotential for water oxidation. Subsequent optimization is required for the anode to decrease the overpotential for water oxidation and further decrease the cell voltage.

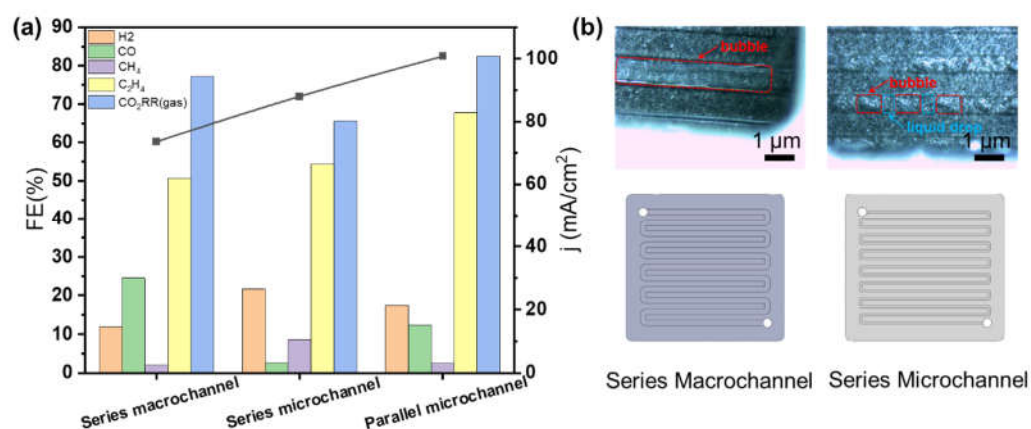


Figure 8. (a) The Faraday efficiency of gas products and current density with different channel structures; (b) microscopic images of the bubble dynamics. Operating parameter: Cell voltage 4.2 V, CO_2 gas flow rate of 10 sccm, anolyte flow rate of 10 sccm, and the anion exchange membrane of Sustainion X37-50 Grade T.

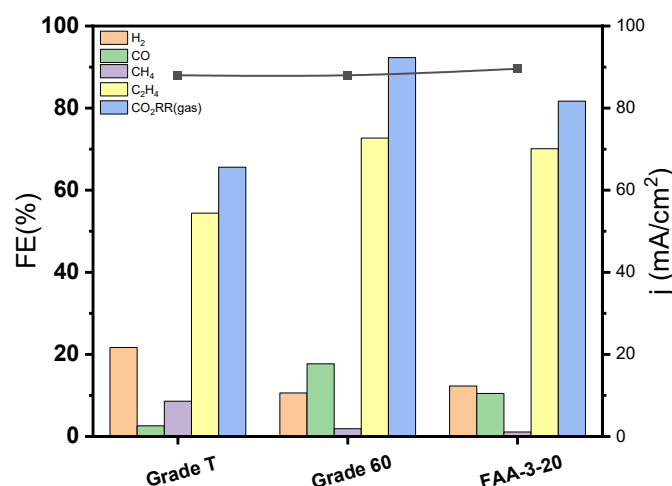


Figure 9. The Faraday efficiency of gas products and current density with different membranes. Operating parameter: Cell voltage 4.2 V, CO_2 gas flow rate of 10 sccm, anolyte flow rate of 10 sccm, and the channel type of series microchannel structure.

2.3.5. Stability

Figure 10 shows the stability test results. Three rounds of tests were conducted, and each test lasted 30 min. The interval between the first test and the second test was 10 min, and the interval between the second test and the third test was 12 h. As shown in Figure 10a, the current was generally stable in the first test and the second test. However, in the third test, the current gradually decreased over time. As shown in Figure 10a, the FEs of H_2 ,

CO, and CH₄ showed no significant difference, and the FEs of C₂H₄ and CO₂RR(gas) even increased. By contrast, the FE of H₂ markedly increased, and the FEs of C₂H₄ and CO₂RR(gas) decreased in the third round. One of the reasons may be attributed to the flooding phenomenon since the hydrophobicity of carbon paper would decrease and the three-phase interface will be damaged when it sets aside for a long time [28,29]. Further, the flooding phenomenon would cause catalysts to fall off from the carbon paper more easily. Parts of the catalysts were found to fall off from the carbon paper and be attached to the anion exchange membranes after the reaction. Figure S4 shows the XRD of CuNWs before and after the reaction. The intensity of the peak at 43.3° decreased, and the peaks at 50.4° and 74.1° disappeared. The decreased intensity was ascribed to the catalyst shedding. No new peaks were found, which demonstrates that the crystal structure of CuNWs remained stable. It is reported that the low stability of Cu-based GDE may originate from the degradation phenomenon [30]. An ICP test was performed to detect the concentrations of Cu and Ir in the anodic solution before and after the reaction (Table S3). The concentrations of both Cu and Ir increased as the reaction time increased, which demonstrates that both anode and cathode showed a degradation phenomenon. In addition, the voltage used in the experiment was relatively high. Carbon paper is easily damaged by high voltage and is susceptible to electrical wetting at high cell voltage [30,31].

On the one hand, continuous material science research is required to develop advanced anode and cathode with low overpotential to decrease the cell voltage. On the other hand, new gas diffusion electrodes other than carbon paper are urgently required, and polytetrafluoroethylene (PTFE)-based gas diffusion electrodes may be good alternatives. However, most of the reported PTFE-based gas diffusion electrodes are based on magnetron sputtering or ion sputtering technology. The combination of nano-synthesis technology and magnetron sputtering technology is expected to play a more considerable role.

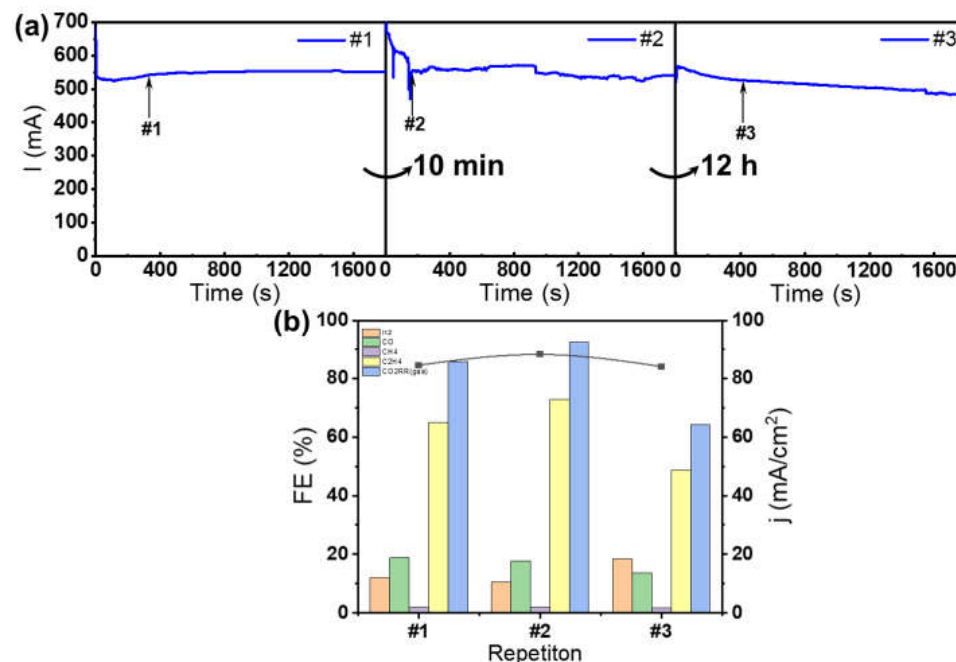


Figure 10. Stability test: (a) I-t curve; (b) the Faraday efficiency and current density. Operating parameter: Cell voltage 4.2 V, CO₂ gas flow rate of 10 sccm, anolyte flow rate of 10 sccm, the anion exchange membrane of Sustainion X37-50 Grade 60, and the channel type of series microchannel structure.

2.3.6. O₂ Production Capability

The oxygen production capability of the membrane reactor is of vital importance for manned spacecraft in the extraterrestrial environment. We measured the oxygen production capability at the condition of cell voltage of 4.2 V, CO₂ gas flow rate of 10 sccm, an

anolyte flow rate of 10 sccm, anion exchange membrane using Sustainion X37-50 Grade 60, and a parallel microchannel structure. The oxygen production capability was 111.7 mg/h (2.68 g/day), and the Faraday efficiency of oxygen was 80.8%. To meet the oxygen requirement, the area of the membrane electrode should be 1900–1960 cm².

3. Materials and Methods

3.1. Materials and Electrode Preparation

CuNWs were prepared according to the previous reference [32]. The catalyst ink was prepared by adding 20 mg CuNWs into a mixed solution of 3 mL cyclohexane and 70 μ L Nafion (DuPont D520, 5 wt%, Suzhou Siner Technology Co., Ltd, China), and then was ultrasonically treated for 60 min to form a homogeneous ink. The GDE was prepared by spraying the above ink with an airbrush on carbon paper (SIGRACET 29BC, Suzhou Siner Technology Co., Ltd, China, 5 cm \times 5 cm). Then, the above GDE was dried by an infrared heat lamp for about 20 min. The catalyst-loading density was about 0.8 mg/cm². Lastly, the GDE was cut to the desired size by using a paper knife.

The IrO₂ based GDE was purchased from Dioxide Materials Inc, Boca Raton, FL, USA.

3.2. Characterization Methods

SEM images were obtained by field emission scanning electron microscopy (Helios G4 CX, Thermo Fisher Scientific, Waltham, MA, USA). TEM images were obtained by using a transmission electron microscope (Tecnai G2 F30, FEI, Hillsboro, OR, USA). XPS spectra were obtained via an X-ray photoelectron spectrometer (ESCALAB 250Xi, Thermo Fisher Scientific, Waltham, MA, USA); all binding energies were corrected according to the C1s peak at 284.8 eV. An X-ray diffractometer (D8 advance, λ = 0.154 nm, Bruker, Billerica, MA, USA) was utilized to observe the XRD patterns. An ICP test was performed through ICP-MS (ICAP-MS-Qc, Thermo Fisher Scientific, Waltham, MA, USA).

3.3. Performance Test

Before the CO₂ reduction experiments, the anion exchange membranes were activated in 1 M KOH and 0.2 M KHCO₃, respectively. Then, the prepared cathode and IrO₂ anode were attached to each side of the anion exchange membrane. Both cathode and anode geometric areas were 2.5 cm \times 2.5 cm. Both the anode and cathode were sealed by the silica gel gasket. The assembled cell was conducted to detect the leakage rate under 0.5 MPa Ar atmosphere.

The CO₂ reduction experiments were performed under potentiostatic operation using a DC power source (B2902A, Keysight Technologies, USA). A DC voltage was supplied on the anodic and cathodic substrates (current collectors), in which the positive electrode was linked to the anode, and the negative one was linked to the cathode, respectively. Then, 0.2 M KHCO₃ aqueous solution was introduced into the anode, and the aqueous solution flow rate was controlled, while CO₂ (99.99%) was continuously purged into the gas channel through a mass flowmeter. After several minutes, until the I-t curve was smooth and steady, 0.25 mL gas products from the reaction were injected into and analyzed by a gas chromatograph (GC-2014C, Shimadzu, Kyoto, Japan), coupled with a thermal conductivity detector (TCD) and a flame ionization detector (FID). For tests at atmosphere conditions, the gas sampling from the soft bag was averaged over the previous time.

4. Conclusions

In this work, we designed an electrochemical membrane reactor at room temperature based on microfluidic control for the reduction of CO₂ in extraterrestrial space. A microfluidic control technique was utilized to promote the gas-liquid interfacial phase separation under a microgravity environment. In this system, the highest Faraday efficiency (FE) of C₂H₄ was 72.7%, with a current density of 88 mA/cm². The single-pass carbon efficiency (SPCE) of CO₂ toward C₂H₄ and gas products were 4.64% and 11.61%, respectively. The CO₂ reduction performance was investigated under different operating conditions

in detail including voltage, the flow rate of electrolyte and CO₂, channel structure, and membrane, respectively. In addition, a microfluidic control technique was adopted to overcome the influence of the microgravity environment. The oxygen production capability was 111.7 mg/h (2.68 g/day). This work provides a possible technology path for CO₂ utilization and O₂ supply during the process of space exploration.

Supplementary Materials: Supporting Information is available online at <https://www.mdpi.com/article/10.3390/catal12010003/s1>, Figure S1: Diameter distributions of CuNWs. Figure S2: XPS of survey spectra of CuNWs. Figure S3: Typical (a) TCD and (b) FID chromatograms of cathodic gas products measured under the condition: CO₂ gas flow rate of 10 sccm, anolyte flow rate of 10 sccm, the voltage of 4.2 V, the anion exchange membrane of Sustainion X37-50 Grade 60, and the channel type of series microchannel structure. Table S1: The single-pass carbon efficiency (SPCE) of CO₂ towards each product at 4.2 V. Table S2: The energy efficiency (EE) of CO₂ towards C₂H₄ at 4.2 V. Table S3: Concentrations of Cu and Ir in the anodic solution before and after the reaction.

Author Contributions: Conceptualization, methodology, visualization, writing—original draft preparation, D.F.; writing—original draft preparation, supervision, validation, investigation, funding acquisition, W.J.; formal analysis, writing—review and editing, C.Z.; L.L.; B.H., and J.S.; project administration, funding acquisition, W.Y. All authors have read and agreed to the published version of the manuscript.

Funding: This work was supported by the National Key Research and Development Program of China (2020YFA0710304), National Natural Science Foundation of China (22002185), Beijing, Natural Science Foundation (2204100), and Outstanding Young Talents Foundation of CAST.

Data Availability Statement: Not applicable.

Conflicts of Interest: The authors declare no conflict of interest.

References

1. Messerschmid, E.; Bertrand, R. *Space Stations: Systems and Utilization*; Springer Science & Business Media: Berlin/Heidelberg, Germany, 2013.
2. Law, J.; Watkins, S.; Alexander, D. In-flight carbon dioxide exposures and related symptoms: Association, susceptibility, and operational implications. *NASA Tech. Paper* **2010**, 216126, 2010.
3. Greenwood, Z.; Abney, M.; Stanley, C.; Brown, B.; Fox, E. State of NASA Oxygen Recovery. In Proceedings of the 48th International Conference on Environmental Systems, Albuquerque, NM, USA, 8–12 July 2018.
4. Hinterman, E.; Hoffman, J.A. Simulating oxygen production on Mars for the Mars Oxygen In-Situ Resource Utilization Experiment. *Acta Astronaut.* **2020**, *170*, 678–685. [[CrossRef](#)]
5. Hecht, M.; Hoffman, J.; Rapp, D.; McClean, J.; SooHoo, J.; Schaefer, R.; Aboobaker, A.; Mellstrom, J.; Hartvigsen, J.; Meyen, F. Mars Oxygen ISRU Experiment (MOXIE). *Space Sci. Rev.* **2021**, *217*, 1–76. [[CrossRef](#)]
6. Yang, L.; Zhang, C.; Yu, X.; Yao, Y.; Li, Z.; Wu, C.; Yao, W.; Zou, Z. Extraterrestrial artificial photosynthetic materials for in-situ resource utilization. *Natl. Sci. Rev.* **2021**, *8*, nwab104. [[CrossRef](#)]
7. Ma, D.; Jin, T.; Xie, K.; Huang, H. An overview of flow cell architectures design and optimization for electrochemical CO₂ reduction. *J. Mater. Chem. A* **2021**, *9*, 20897–20918. [[CrossRef](#)]
8. O'Brien, C.P.; Miao, R.K.; Liu, S.; Xu, Y.; Lee, G.; Robb, A.; Huang, J.E.; Xie, K.; Bertens, K.; Gabardo, C.M. Single Pass CO₂ Conversion Exceeding 85% in the Electrosynthesis of Multicarbon Products via Local CO₂ Regeneration. *ACS Energy Lett.* **2021**, *6*, 2952–2959. [[CrossRef](#)]
9. Gabardo, C.M.; O'Brien, C.P.; Edwards, J.P.; McCallum, C.; Xu, Y.; Dinh, C.-T.; Li, J.; Sargent, E.H.; Sinton, D. Continuous carbon dioxide electroreduction to concentrated multi-carbon products using a membrane electrode assembly. *Joule* **2019**, *3*, 2777–2791. [[CrossRef](#)]
10. Dunfeng, G.; Pengfei, W.; Hefei, L.; Long, L.; Guoxiong, W.; Xinhe, B. Designing Electrolyzers for Electrocatalytic CO₂ Reduction. *Acta Phys.-Chim. Sin.* **2021**, *37*, 2009021-0.
11. Luo, Y.; Zhang, K.; Li, Y.; Wang, Y. Valorizing carbon dioxide via electrochemical reduction on gas-diffusion electrodes. *InfoMat* **2021**, 1–20. [[CrossRef](#)]
12. Lee, W.H.; Kim, K.; Lim, C.; Ko, Y.-J.; Hwang, Y.J.; Min, B.K.; Lee, U.; Oh, H.-S. New strategies for economically feasible CO₂ electroreduction using a porous membrane in zero-gap configuration. *J. Mater. Chem. A* **2021**, *9*, 16169–16177. [[CrossRef](#)]
13. Wei, P.; Li, H.; Lin, L.; Gao, D.; Zhang, X.; Gong, H.; Qing, G.; Cai, R.; Wang, G.; Bao, X. CO₂ electrolysis at industrial current densities using anion exchange membrane based electrolyzers. *Sci. China Chem.* **2020**, *63*, 1711–1715. [[CrossRef](#)]
14. Vennekoetter, J.-B.; Sengpiel, R.; Wessling, M. Beyond the catalyst: How electrode and reactor design determine the product spectrum during electrochemical CO₂ reduction. *Chem. Eng. J.* **2019**, *364*, 89–101. [[CrossRef](#)]

15. Matsushima, H.; Nishida, T.; Konishi, Y.; Fukunaka, Y.; Ito, Y.; Kuribayashi, K. Water electrolysis under microgravity: Part 1. Experimental technique. *Electrochim. Acta* **2003**, *48*, 4119–4125. [[CrossRef](#)]
16. Modestino, M.A.; Rivas, D.F.; Hashemi, S.M.H.; Gardeniers, J.G.E.; Psaltis, D. The potential for microfluidics in electrochemical energy systems. *Energy Environ. Sci.* **2016**, *9*, 3381–3391. [[CrossRef](#)]
17. Jiang, W.; Ruan, Q.; Xie, J.; Chen, X.; Zhu, Y.; Tang, J. Oxygen-doped carbon nitride aerogel: A self-supported photocatalyst for solar-to-chemical energy conversion. *Appl. Catal. B Environ.* **2018**, *236*, 428–435. [[CrossRef](#)]
18. Gu, Z.; Yang, N.; Han, P.; Kuang, M.; Mei, B.; Jiang, Z.; Zhong, J.; Li, L.; Zheng, G. Oxygen vacancy tuning toward efficient electrocatalytic CO₂ reduction to C₂H₄. *Small Methods* **2019**, *3*, 1800449.
19. Li, M.; Ma, Y.; Chen, J.; Lawrence, R.; Luo, W.; Sacchi, M.; Jiang, W.; Yang, J. Residual Chlorine Induced Cationic Active Species on a Porous Copper Electrocatalyst for Highly Stable Electrochemical CO₂ Reduction to C²⁺. *Angew. Chem.* **2021**, *133*, 11588–11594. [[CrossRef](#)]
20. Li, R.; Xu, J.; Zeng, R.; Pan, Q.; Tang, T.; Luo, W. Halides-assisted electrochemical synthesis of Cu/Cu₂O/CuO core-shell electrocatalyst for oxygen evolution reaction. *J. Power Sources* **2020**, *457*, 228058. [[CrossRef](#)]
21. Weekes, D.M.; Salvatore, D.A.; Reyes, A.; Huang, A.; Berlinguette, C.P. Electrolytic CO₂ reduction in a flow cell. *Accounts. Chem. Res.* **2018**, *51*, 910–918. [[CrossRef](#)] [[PubMed](#)]
22. Xu, Y.; Edwards, J.P.; Liu, S.; Miao, R.K.; Huang, J.E.; Gabardo, C.M.; O'Brien, C.P.; Li, J.; Sargent, E.H.; Sinton, D. Self-cleaning CO₂ reduction systems: Unsteady electrochemical forcing enables stability. *ACS Energy Lett.* **2021**, *6*, 809–815. [[CrossRef](#)]
23. Endrődi, B.; Samu, A.; Kecsenovity, E.; Halmágyi, T.; Sebők, D.; Janáky, C. Operando cathode activation with alkali metal cations for high current density operation of water-fed zero-gap carbon dioxide electrolyzers. *Nat. Energy* **2021**, *6*, 439–448. [[CrossRef](#)]
24. Huang, J.E.; Li, F.; Ozden, A.; Rasouli, A.S.; de Arquer, F.P.G.; Liu, S.; Zhang, S.; Luo, M.; Wang, X.; Lum, Y. CO₂ electrolysis to multicarbon products in strong acid. *Science* **2021**, *372*, 1074–1078. [[CrossRef](#)] [[PubMed](#)]
25. Xing, Z.; Hu, L.; Ripatti, D.S.; Hu, X.; Feng, X. Enhancing carbon dioxide gas-diffusion electrolysis by creating a hydrophobic catalyst microenvironment. *Nat. Commun.* **2021**, *12*, 1–11. [[CrossRef](#)]
26. Endrődi, B.; Kecsenovity, E.; Samu, A.; Halmágyi, T.; Rojas-Carbonell, S.; Wang, L.; Yan, Y.; Janáky, C. High carbonate ion conductance of a robust PiperION membrane allows industrial current density and conversion in a zero-gap carbon dioxide electrolyzer cell. *Energ. Environ. Sci.* **2020**, *13*, 4098–4105. [[CrossRef](#)]
27. Salvatore, D.A.; Gabardo, C.M.; Reyes, A.; O'Brien, C.P.; Holdcroft, S.; Pintauro, P.; Bahar, B.; Hickner, M.; Bae, C.; Sinton, D. Designing anion exchange membranes for CO₂ electrolyzers. *Nat. Energy* **2021**, *6*, 339–348. [[CrossRef](#)]
28. Shi, R.; Guo, J.; Zhang, X.; Waterhouse, G.I.; Han, Z.; Zhao, Y.; Shang, L.; Zhou, C.; Jiang, L.; Zhang, T. Efficient wettability-controlled electroreduction of CO₂ to CO at Au/C interfaces. *Nat. Commun.* **2020**, *11*, 1–10. [[CrossRef](#)] [[PubMed](#)]
29. Chen, S.; Li, W.-H.; Jiang, W.; Yang, J.; Zhu, J.; Wang, L.; Ou, H.; Zhuang, Z.; Chen, M.; Sun, X. MOF Encapsulating N-Heterocyclic Carbene-Ligated Copper Single-Atom Site Catalyst towards Efficient Methane Electrosynthesis. *Angew. Chem. Int. Edit.* **2021**. [[CrossRef](#)]
30. Popović, S.; Smiljanić, M.; Jovanović, P.; Vavra, J.; Buonsanti, R.; Hodnik, N. Stability and Degradation Mechanisms of Copper-Based Catalysts for Electrochemical CO₂ Reduction. *Angew. Chem. Int. Edit.* **2020**, *59*, 14736–14746. [[CrossRef](#)] [[PubMed](#)]
31. Yang, K.; Kas, R.; Smith, W.A.; Burdyny, T. Role of the carbon-based gas diffusion layer on flooding in a gas diffusion electrode cell for electrochemical CO₂ reduction. *ACS Energy Lett.* **2020**, *6*, 33–40. [[CrossRef](#)]
32. Choi, C.; Kwon, S.; Cheng, T.; Xu, M.; Tieu, P.; Lee, C.; Cai, J.; Lee, H.M.; Pan, X.; Duan, X. Highly active and stable stepped Cu surface for enhanced electrochemical CO₂ reduction to C₂H₄. *Nat. Catal.* **2020**, *3*, 804–812. [[CrossRef](#)]